Liquid-vapor interface of the Stockmayer fluid in a uniform external field

Stan G. Moore,* Mark J. Stevens, and Gary S. Grest
Sandia National Laboratories, Albuquerque, New Mexico 87185, USA
(Received 23 December 2014; published 23 February 2015)

The effect of a uniform (nonspatially varying) external field on the liquid-vapor interface of the Stockmayer fluid (Lennard-Jones particles embedded with a point dipole) has been investigated by molecular-dynamics simulations. The long-ranged parts of both the dipole and Lennard-Jones interactions are treated using an Ewald summation, which removes the effects of the cutoff. The direction of the field shifts the critical point and interfacial properties in different directions. For an external field parallel to the interface, the critical temperature increases, while for a field applied perpendicular to the interface, it decreases. The effects of the field on surface tension and interfacial width are also investigated. For zero field, dipoles near the liquid-vapor interface show a weak orientation parallel to the interface. For fields parallel to the interface, ordering in the liquid phase is greater than the vapor, while for fields perpendicular to the interface, the opposite is true.

DOI: 10.1103/PhysRevE.91.022309 PACS number(s): 64.70.F−, 68.03.Cd, 75.50.Mm, 77.22.−d

I. INTRODUCTION

Dipolar fluids have many additional characteristics compared to simple liquids that have important consequences in the statistical physics of these fluids. For large dipole moments, the liquid can become ordered even in the absence of an external field [1]. The presence of an external field brings an additional control that can be used to switch or modify the statistical states of the fluid. Liquid-vapor coexistence is a key aspect of the phase diagram of any liquid, and there has been much interest in liquid-vapor coexistence in dipolar systems in an external field both experimentally [2–6] and theoretically [5,7–21].

Experimental measurements of the change in the critical temperature in the presence of an electric field on various dipolar molecular systems have produced varying results. Several experiments have found that the presence of an electric field leads to a decrease in critical temperature of binary mixtures [2,3,5]. Beaglehole found the change in critical temperature for a mixture of cyclohexane and aniline depends on the field direction; the critical temperature increases for the field perpendicular to the interface, and decreases with the field parallel to the interface [4]. However, Hegseth and Kamel found an increase in critical temperature for an alternating current electric field applied to a spherical capacitor filled with pure SF_6 at its critical density [6].

Theoretical calculations of the change in critical temperature of dipolar fluids due to an electric field depend on the boundary conditions. Landau and Lifsitz showed that the electrostatic thermodynamic potential is different in the case of a constant surface charge compared to a constant surface potential [7]. This difference leads to a reversal of the sign of the predicted shift of the critical temperature. Samin and Tsori using van der Waal's theory and Onsager's dieletric theory treated the vapor-liquid coexistence of polar and nonpolar fluids in the presence of a nonuniform electric field [9]. They found for constant surface potential, the surface tension and hence the critical temperature increases compared to the zero-field case, while for constant surface charge, the critical temperature decreases. Mean-field theory predicts that the sign of the critical temperature shift also depends on the second derivative of the dielectric constant with respect to composition (i.e., density for a pure fluid), which for most fluids is positive [8]. This leads to an increase of critical temperature for constant surface potential [5]. Stepanow and Thurn-Albrecht formulated a statistical mechanical description of liquid systems for polar systems in an electric field with constant potential boundary conditions and also found that the field induced a postive shift of the critical temperature for polar liquids [10]. Warshavsky and Zeng explicitly treated the liquid-vapor interface using density-functional theory [19] and found the critical temperature increases for a field applied parallel to the interface, and decreases for a field perpendicular to the interface. This suggests that a parallel field is equivalent to the constant surface potential boundary condition.

Several simulations using a variety of methods and systems have been performed. A canonical dipolar system to study has been the Stockmayer fluid, which is Lennard-Jones particles with fixed-point dipoles [22]. Many simulations of the critical behavior have used the Gibbs ensemble method, which separately treats the liquid and vapor phases without an interface. Consequently, the orientation of the field relative to the interface is not explicitly defined. For both Stockmayer fluids and realistic fluids, the Gibbs ensemble simulations found that the critical temperature is increased in the presence of an electric field [12,14–16,18]. Srivastava *et al.*, using molecular-dynamics (MD) simulations, found that the critical temperature of bulk water increased, while for confined water it decreased in the presence of an electric field parallel to the interface [11]. Jia and Hentschke used single-phase MD simulations and the Maxwell equal-area construction to obtain the critical point of the Stockmayer fluid [21]. They used a reaction field method with an external field applied using the two standard boundary conditions: constant potential and constant surface charge. As in the above theories, they found the critical temperature increases in the constant potential case and decreases for constant surface charge.

Our focus is on the most commonly treated dipolar system, the Stockmayer potential. We study the liquid-vapor interface explicitly for a 3D Stockmayer fluid in a uniform external field. We calculate coexistence curves, orientation profiles, surface tension, and interfacial width, and determine the effect of the

*stamoor@sandia.gov

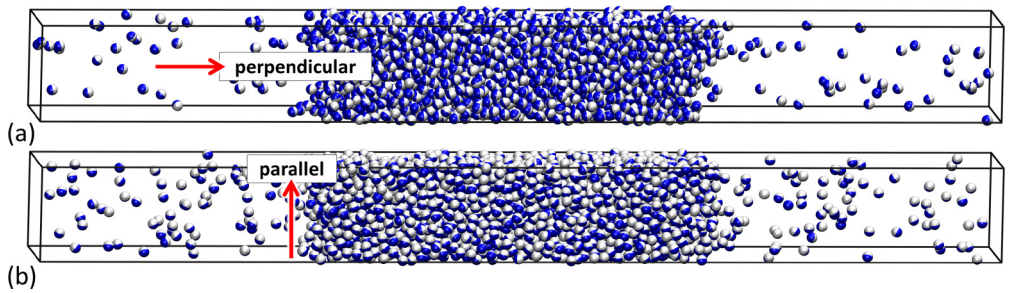

FIG. 1. (Color online) Snapshot of the Stockmayer liquid-vapor interface for (a) $\mu^* = 0.5$, $T^* = 0.8$, and $E^*_\perp = 10.0$, and for (b) $\mu^* = 0.5$, $T^* = 1.0$, and $E^*_\parallel = 10.0$. The direction of the external field in relation to the interface is also shown. Dipoles are represented as dual colored spheres, where the dipole points from blue to white.

field strength and direction on these properties. We first present in the next section an overview of the simulation methods, and then present results for the effect of different field directions on the Stockmayer fluid for a range of dipole moments and field strength.

II. SIMULATION METHODS AND THEORY

The Stockmayer fluid consists of Lennard Jones (LJ) interactions with a point dipole. The LJ potential is

$$U_{\mathrm{LJ}}(r) = 4\varepsilon\left[\left(\frac{\sigma}{r}\right)^{12} - \left(\frac{\sigma}{r}\right)^{6}\right], \tag{1}$$

where σ and ε are the LJ distance and energy parameters and $r = r_{ij} = |\mathbf{r}_i - \mathbf{r}_j|$ is the intermolecular distance between particles i and j. Note that we use a different epsilon symbol, ϵ, for the dielectric constant.

The dipolar potential is [23]

$$U_{\mathrm{dipole}}(r) = \frac{\boldsymbol{\mu}_i \cdot \boldsymbol{\mu}_j}{r_{ij}^3} - 3\frac{(\boldsymbol{\mu}_i \cdot \mathbf{r}_{ij})(\boldsymbol{\mu}_j \cdot \mathbf{r}_{ij})}{r_{ij}^5}, \tag{2}$$

where $\boldsymbol{\mu}_i$ is the point dipole of particle i. Expressions for the forces, torques, and pressure of the Stockmayer fluid can be found in the literature [23–25]. LJ units are used throughout this work and are denoted with a superscript asterisk. The LJ reduced dipole moment is $\mu^* = \mu/\sqrt{\varepsilon\sigma^3}$, and the LJ reduced external field is $E^* = E\sqrt{\sigma^3/\varepsilon}$.

In the presence of a uniform (nonspatially varying) external electric field $\mathbf{E}^{\mathrm{ext}}$, an external torque $\mathbf{T}_i^{\mathrm{ext}}$ acts on the dipoles as

$$\mathbf{T}_i^{\mathrm{ext}} = \boldsymbol{\mu}_i \times \mathbf{E}^{\mathrm{ext}}, \tag{3}$$

which tends to align the dipoles with the external field. Because the external field is uniform, no net force is produced on the dipoles.

The long-ranged nature of the dipolar interaction can present computational challenges in analytic methods and simulations [26]. The dipolar interactions decay as r^{-3} and are therefore long-ranged and only conditionally convergent. To treat the r^{-3} interaction, we use a lattice (Ewald) sum for point dipoles [23–25,27], along with conducting (tinfoil) boundary conditions. It is also necessary to include a 2D slab correction [28,29] for the case of a field applied perpendicular to the interface (see the Appendix A for more details). Alternatively, one can use the reaction field method [30,31] to treat the long-range dipole interactions, which is computationally more efficient but less rigorous than the Ewald sum method. In this work, the LJ dispersion (r^{-6}) interaction is also treated using an Ewald sum [32–34], which eliminates effects of a finite cutoff on the liquid-vapor coexistence curve and on the interfacial properties such as the surface tension [35,36]. For the Ewald sum, the real-space cutoff for both LJ and dipoles was 7.5σ, and other parameters were adjusted to give a root-mean-square (rms) force error of approximately 10^{-4} based on formulas given in Ref. [23], relative to a force of 1.0 in LJ units.

The simulation cell lengths were $L_x^* = L_y^* = 10$ and $L_z^* = 10L_x^*$. The number of particles was 2992 for $\mu^* = 2.0$ and 3000 for all other values of μ^*. The liquid-vapor interface is in the x-y plane, normal to the z direction. A snapshot of the liquid-vapor interface for $\mu^* = 0.5$ and $E^* = 10.0$ is shown in Fig. 1. The external field direction in relation to the interface is also shown for the field parallel ($E_\parallel$) and perpendicular ($E_\perp$) to the interface.

For ease of postprocessing, the density histogram was shifted until the liquid phase was centered in the z direction at $L_z/2$. The density profile was fit using [36,37]

$$\rho(z) = \rho_{\mathrm{gas}} + 0.5(\rho_{\mathrm{liq}} - \rho_{\mathrm{gas}})\left\{\mathrm{erf}\left[\frac{\sqrt{\pi}}{w}(z - 0.5L_z + z_0)\right] - \mathrm{erf}\left[\frac{\sqrt{\pi}}{w}(z - 0.5L_z - z_0)\right]\right\}, \tag{4}$$

which takes into account that two interfaces are formed. The parameters ρ_{liq}, ρ_{vap}, w, and z_0 are obtained from the fit, where ρ_{liq} and ρ_{vap} are the liquid and vapor coexistence densities, w is related to the interfacial width Δ as [36]

$$\Delta^2 = \frac{w^2}{2\pi}, \tag{5}$$

and $L_z/2 \pm z_0$ is the location of the interface. We note that while the density profile can be fit using a hyperbolic tangent function (corresponding to the mean-field result), the error function is more theoretically justified [36].

For a planar interface (normal to the z direction), the surface tension γ can be obtained from the diagonal components of the pressure tensor $\mathbf{P}$ [36,38] as

$$\gamma = \frac{L_z}{2}\left[\langle P_{zz}\rangle - \tfrac{1}{2}(\langle P_{xx}\rangle + \langle P_{yy}\rangle)\right], \tag{6}$$

where $\langle\cdots\rangle$ denotes the time average, and a factor of 1/2 is included because two interfaces are formed.

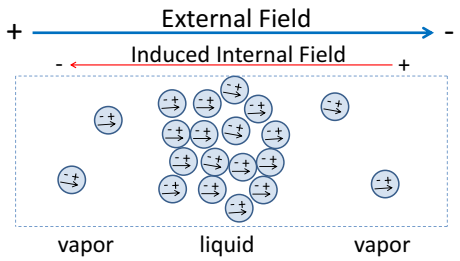

FIG. 2. (Color online) Conceptual diagram of the polarization that occurs when an external field is applied perpendicular to the interface.

For an external field applied perpendicular to the interface, polarization occurs due to the change in density (in the z direction) of the liquid-vapor interface as shown in Fig. 2. This polarization produces a field $\mathbf{E}^{\text{pol}}$ that opposes the applied external field, and the effective external field $\mathbf{E}^{\text{eff}}$ is less than the applied $\mathbf{E}^{\text{ext}}$, related to the dielectric constant ϵ:

$$\mathbf{E}^{\text{eff}} = \mathbf{E}^{\text{ext}} - \mathbf{E}^{\text{pol}} = \mathbf{E}^{\text{ext}}/\epsilon. \tag{7}$$

Note that this definition of *polarization* is similar to that of a dielectric material inside a parallel-plate capacitor. There are no induced dipoles in the Stockmayer system as all point dipoles are fixed magnitude (i.e., permanent).

The static dielectric constant of a polar fluid can be calculated as [27]

$$\epsilon = 1 + \tfrac{4}{3}\pi V^{-1}\beta(\langle \mathbf{M}^2\rangle - \langle \mathbf{M}\rangle^2), \tag{8}$$

where V is the system volume, $\beta = 1/(k_{\text{B}}T)$, where k_{B} is Boltzmann's constant, T is the system temperature, and $\mathbf{M}$ is the total dipole moment of the system:

$$\mathbf{M} = \sum_{i=1}^{N} \boldsymbol{\mu}_i. \tag{9}$$

We note that Eq. (8) assumes conducting (tinfoil) boundary conditions for the Ewald sum.

A position-dependent dipole orientation parameter $\cos\theta(z)$ was calculated, where $\theta(z)$ is the angle between the dipole moment at position z and the unit vector parallel to the field (not the interface). Using the definition of the scalar product, one can express $\cos\theta(z)$ for the field applied perpendicular to the plane of the interface (i.e., applied in the z direction) as

$$\cos\theta(z) = L_z \sum_{i=1}^{N} \frac{\mu_{z,i}}{\mu_i}\delta(z - z_i), \tag{10}$$

where δ is the Dirac δ and $\mu_{z,i}$ is the z component of $\boldsymbol{\mu}_i$. If all dipoles are aligned parallel to the field, then $\cos\theta(z) = 1$. If all dipoles are aligned perpendicular to the field or are randomly aligned, then $\cos\theta(z) = 0$. Similarly, for the field applied parallel to the plane of the interface (i.e., applied in the y direction)

$$\cos\theta(z) = L_z \sum_{i=1}^{N} \frac{\mu_{y,i}}{\mu_i}\delta(z - z_i). \tag{11}$$

The average second Legendre polynomial $P_2(z)$ of orientation [39–41] can also be calculated as

$$P_2(z) = \tfrac{1}{2}\langle 3\,\cos^2\theta(z) - 1\rangle. \tag{12}$$

If all dipoles are aligned parallel to the field, then $P_2(z) = 1$. If all dipoles are aligned perpendicular to the field, $P_2(z) = -\frac{1}{2}$, and if they are randomly aligned, then $P_2(z) = 0$. For simulations with zero field, $\cos\theta(z)$ and $P_2(z)$ were computed using Eq. (10). We found that an error function fit similar to Eq. (4) also worked well for $\cos\theta(z)$ and $P_2(z)$ [i.e., replacing density with orientation in Eq. (4)], which gave the average orientation in the liquid and vapor phases. In practice, $\rho(z)$, $\cos\theta(z)$, and $P_2(z)$ were calculated as histograms using 100 bins in the z direction.

The MD simulations were performed using LAMMPS [42]. The time step of $\Delta t = 0.002\tau$, where $\tau = \sigma\sqrt{(m/\epsilon)}$. A Langevin thermostat [43,44] was used to control both the translational and rotational temperatures, with a damping constant of $1.0/\tau$. The liquid-vapor interface was formed by placing a slab of liquidlike density on a face-centered-cubic (fcc) lattice surrounded by slabs of vaporlike density (also on an fcc lattice) in the z direction. The system was briefly relaxed by minimizing the potential energy and then allowed to equilibrate by running with dynamics. After equilibration, production simulations were then run 2000τ.

During the simulations, the center of mass of the system was held fixed to prevent the interface from drifting, and the total linear and rotational momentum of the system were zeroed every 2τ. The LAMMPS option to zero out the total force from the Langevin thermostat was used.

III. RESULTS AND DISCUSSION

A. Coexistence in an external field

For dipole moments $0 \leqslant \mu^* \leqslant 2.5$, a series of two-phase simulations were performed to calculate the coexistence data for field strengths in the range $0 \leqslant E^* \leqslant 10.0$. The density profile at each temperature was fit using Eq. (4) to obtain coexistence densities ρ_{gas} and ρ_{liq} and interfacial width Δ as shown in Fig. 3(a). Applying the external field parallel to the interface lowers the liquid density and raises the vapor density, while the opposite happens when the field is applied perpendicular to the interface.

The coexistence curve for $\mu^* = 1.0$ for zero field and for $E^* = 2.0$ is shown in Fig. 4(a). The critical point was fit using the law of rectilinear diameters [45] and the universal Ising critical exponent $\beta = 0.326$ [46]. For $E^* = 0$ and $\mu^* = 1.0$, $T_{\text{c}}^* = 1.415$ and $\rho_{\text{c}}^* = 0.309$, which agree well with GEMC results reported by van Leeuwen and Smit [47]: $T_{\text{c}}^* = 1.41 \pm 0.01$ and $\rho_{\text{c}}^* = 0.30 \pm 0.01$. Applying the external field parallel to the interface increases the critical temperature, while applying the field perpendicular to the interface decreases the critical temperature as shown in Fig. 4, which is in agreement with DFT calculations [19].

Results for several different dipole moments μ^* and external field strengths E^* are shown in Table I. Interestingly, for $\mu^* = 1.0$, the magnitude of the shift of the critical temperature due to the two-field directions is approximately equal as shown in Fig. 4(a). For $\mu^* > 1.0$, the effect of the parallel field on T_{c} is greater than that of the perpendicular field as shown in

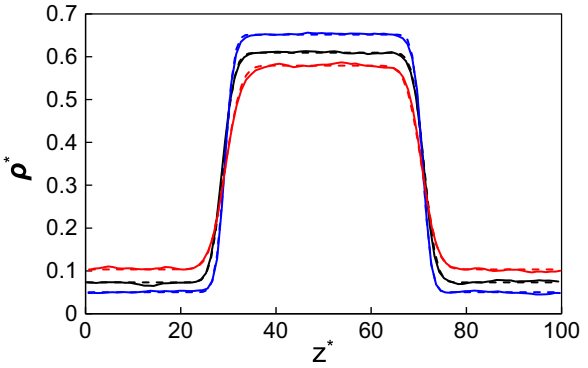

FIG. 3. (Color online) Density profiles of the Stockmayer fluid for $\mu^* = 1.0$, $T^* = 1.25$ for zero field (black line, middle curve), external field parallel to the interface $E_\parallel^* = 2.0$ (red line, lower curve in liquid phase), and external field perpendicular to the interface $E_\perp^* = 2.0$ (blue line, upper curve in liquid phase). Solid lines represent the data and dashed lines represent a fit of the data using Eq. (4).

Fig. 4(b) and, for $\mu^* < 1.0$, the opposite is true as shown in Table I. The critical density is increased for perpendicular field, while for parallel field, little change is seen as shown in Fig. 4 and Table I.

To quantify the uncertainty in the results, simulations to obtain the critical-point shift were repeated for a low dipole moment, low field strength point, and for a high dipole, high field strength point: for $\mu^* = 1.0$ and $E^* = 1.0$, and for $\mu^* = 2.5$ and $E^* = 3.2$. These simulations were run for 2000τ, and were broken into four blocks which were used to calculate 95% confidence intervals based on the Student's t distribution. For $\mu^* = 1.0$ and $E_\parallel^* = 1.0$, $\Delta T_c^* = 0.017 \pm 0.010$ and $\Delta\rho_c^* = 0.001 \pm 0.012$, while for $E_\perp^* = 1.0$, $\Delta T_c^* = -0.023 \pm 0.011$ and $\Delta\rho_c^* = 0.001 \pm 0.010$. For $\mu^* = 2.5$ and $E_\parallel^* = 3.2$, $\Delta T_c^* = 0.427 \pm 0.015$ and $\Delta\rho_c^* = 0.000 \pm 0.008$, while for $E_\perp^* = 3.2$, $\Delta T_c^* = -0.211 \pm 0.032$ and $\Delta\rho_c^* = 0.082 \pm 0.004$. The direction of the shift in critical temperature is statistically significant in all of these cases. The shift in critical density is typically so small and is not statistically significant, except for the high field and dipole moment case of $\mu^* = 2.5$ and $E_\perp^* = 3.2$. We also note that while using the universal Ising critical exponent to fit critical-point data should give results that are not highly dependent on the finite size of the system [27], a more sophisticated finite-size scaling method to obtain the critical point in the thermodynamic limit (not used in this work) has been developed [48–51].

TABLE I. Critical-point data.

μ^*	$E_\parallel^*$	$E_\perp^*$	T_c^*	ΔT_c^*	ρ_c^*	$\Delta\rho_c^*$
0.5	0.0	0.0	1.309		0.311	
0.5	6.0	0.0	1.352	0.043	0.302	−0.009
0.5	0.0	6.0	1.231	−0.078	0.319	0.008
0.5	10.0	0.0	1.369	0.060	0.309	−0.002
0.5	0.0	10.0	1.183	−0.126	0.312	0.001
1.0	0.0	0.0	1.415		0.309	
1.0	1.0	0.0	1.430	0.015	0.312	0.003
1.0	0.0	1.0	1.390	−0.025	0.317	0.008
1.0	2.0	0.0	1.471	0.056	0.312	0.003
1.0	0.0	2.0	1.352	−0.063	0.327	0.018
1.0	2.0	2.0	1.423	0.008	0.323	0.014
2.0	0.0	0.0	2.066		0.285	
2.0	1.5	0.0	2.243	0.177	0.289	0.004
2.0	0.0	1.5	2.016	−0.050	0.302	0.017
2.5	0.0	0.0	2.602		0.269	
2.5	2.0	0.0	2.906	0.304	0.270	0.001
2.5	0.0	2.0	2.489	−0.113	0.314	0.045
2.5	3.2	0.0	3.026	0.424	0.266	−0.003
2.5	0.0	3.2	2.395	−0.207	0.355	0.086
2.5	5.0	0.0	3.224	0.622	0.266	−0.003

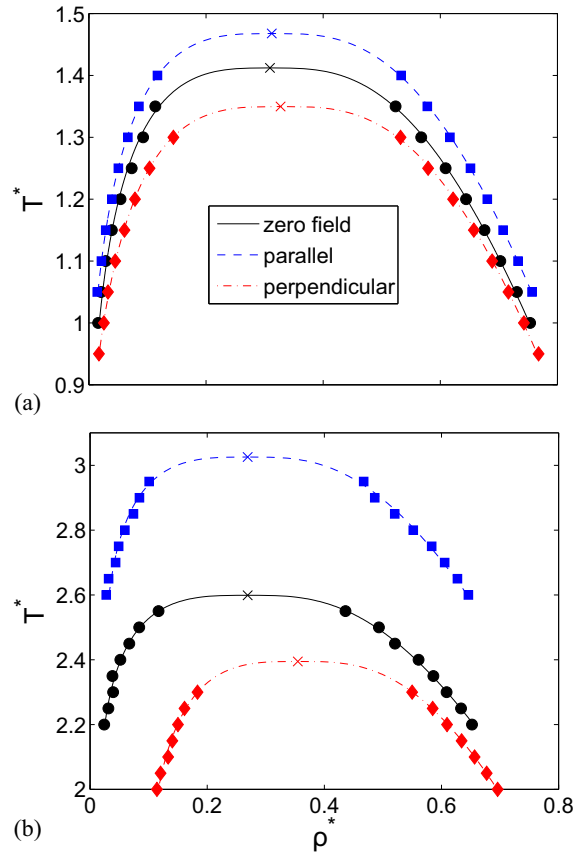

FIG. 4. (Color online) Phase coexistence curves of the Stockmayer fluid for (a) $E^* = 0$ and 2.0 and $\mu^* = 1.0$ and (b) $E^* = 0$ and 3.2 and $\mu^* = 2.5$.

Our results for ΔT_c^* can be compared to other calculations for the Stockmayer fluid in an external field. Figure 5 shows the field dependence for three values of μ^*. Most of the data points are in agreement. There is more data with positive ΔT_c^*, because the data from Monte Carlo simulations only yields the constant potential boundary condition, which has $\Delta T_c^* > 0$. The agreement between our data with the field parallel to the interface and the other data with constant surface potential boundary condition implies that the two cases are equivalent. While there is less data for the perpendicular field and constant surface charge, the data suggests that these two are equivalent. The foundation for this is in the polarization of the dipoles as discussed below. For $E^* = 5.0$, our results for ΔT_c^* are 19% higher than those of Ref. [16] and 44% lower than the mean-field result in Ref. [21], as shown in Fig. 5(c). At this

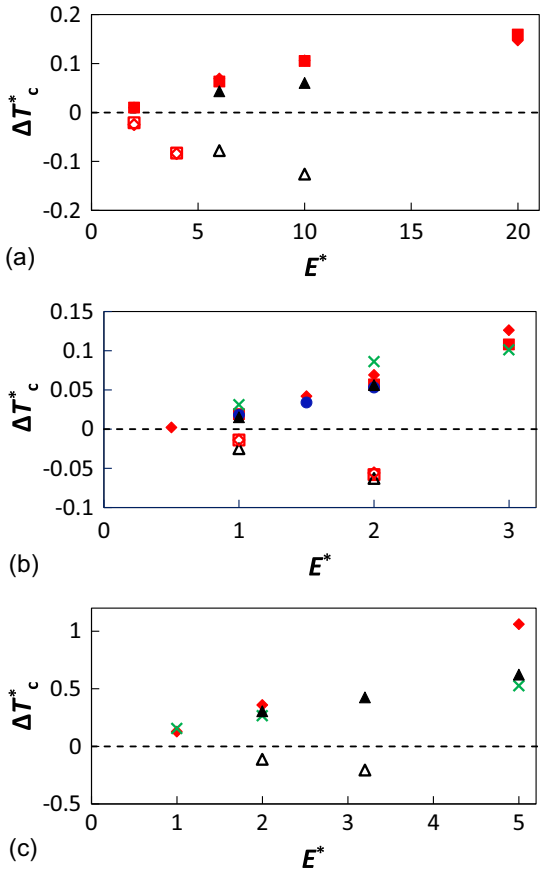

FIG. 5. (Color online) Shift in critical temperature ΔT_c^* vs field strength E^* for Stockmayer fluid at (a) $\mu^* = 0.5$, (b) $\mu^* = 1.0$, and (c) $\mu^* = 2.5$. Black triangles represent simulation results from this work, red squares and diamonds represent simulation and mean-field results, respectively, from Ref. [21], and additional simulation results are also shown as blue circles (Ref. [14]) and green crosses (Ref. [16]). Open triangles, diamonds, and squares represent perpendicular field (i.e., $\Delta T_c^* < 0$), while all other symbols represent parallel field.

large dipole moment and field strength, it is not surprising that the mean-field approximation fails.

Jia and Hentschke used single-phase MD simulations and the Maxwell equal-area construction to obtain critical points of the Stockmayer fluid [21]. This requires homogeneous simulations at thermodynamically metastable and unstable conditions. With this method, it is necessary to use small simulation sizes to prevent phase separation; the size of the simulation box must be smaller than the spatial scale of density fluctuations [52]. Jia and Hentschke found that for constant surface charge boundary conditions using a large field led to inhomogeneities. Since we include the interface explicitly, we can simulate larger perpendicular fields. However, we note that for $\mu^* = 2.5$ with $E_\perp^* = 5.0$, we were also unable to form a distinct liquid-vapor interface as the simulations consisted entirely of interfacial region without a strong separation between the two phases.

For $E_\parallel$, a relative critical temperature T_c^E is defined as

$$T_{c,\parallel}^E = \frac{T_c(E_\parallel)}{T_c(0)}, \tag{13}$$

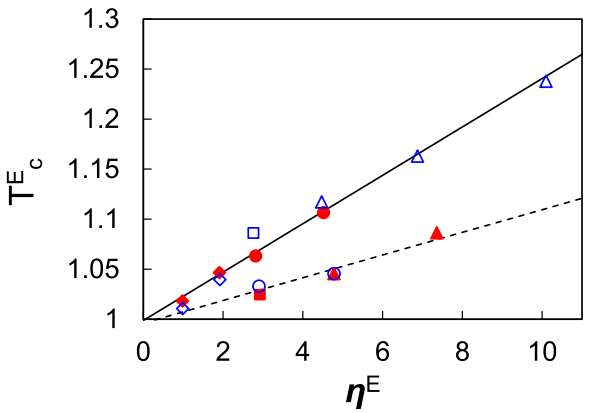

FIG. 6. (Color online) Relative critical temperature T_c^E vs dimensionless field η^E for $\mu^* = 0.5$ (circles), $\mu^* = 1.0$ (diamonds), $\mu^* = 2.0$ (squares), and $\mu^* = 2.5$ (triangles). Blue open symbols represent parallel field, and red closed symbols represent perpendicular field. The solid line is a least-squares fit of the data including $\mu^* \geqslant 1.0$ with parallel field, $\mu^* \leqslant 1.0$ with perpendicular field, and the zero-field case. The dashed line is a least-squares fit to the data including $\mu^* > 1.0$ with perpendicular field, $\mu^* < 1.0$ with parallel field, and the zero-field case.

where $T_c(E)$ is the critical temperature at field strength E, and $T_c(0)$ is the critical point for zero field [16]. For $E_\perp$, the critical point is decreased, so we define the relative critical temperature as

$$T_{c,\perp}^E = \frac{T_c(0)}{T_c(E_\perp)}, \tag{14}$$

so that T_c^E is always greater than one. The data in Table I collapses by using a dimensionless field defined for parallel field as

$$\eta_\parallel^E = \frac{\mu E_\parallel}{T_{c,\parallel}^E}, \tag{15}$$

and for perpendicular field as

$$\eta_\perp^E = \frac{\mu E_\perp}{T_{c,\perp}^E}. \tag{16}$$

The effect of dipole strength and external field on T_c are shown in Fig. 6. The results for $\mu^* \geqslant 1.0$ and parallel field roughly match the results for $\mu^* \leqslant 1.0$ and perpendicular field when $\eta_\parallel^E = \eta_\perp^E$. Similarly, the results for $\mu^* \geqslant 1.0$ and perpendicular field roughly match the results for $\mu^* \leqslant 1.0$ and parallel field when $\eta_\parallel^E = \eta_\perp^E$, though the slope of the solid line is 2.13 times greater than the slope of the dashed line. We note that the results in Fig. 6 for $\mu^* \geqslant 1.0$ with parallel field can be directly compared to results for GEMC simulations shown in Fig. 5 of Ref. [16].

Another interesting case is when the external field has both a parallel and perpendicular component, and there is a competing effect on the critical point; the parallel field increases T_c and the perpendicular field decreases T_c. For $\mu^* = 1.0$ and $E_\parallel^* = E_\perp^* = 2.0$, this effect is approximately equal, and there is little change on T_c as shown in Table I. However, the phase coexistence curve is broadened relative to the zero-field case.

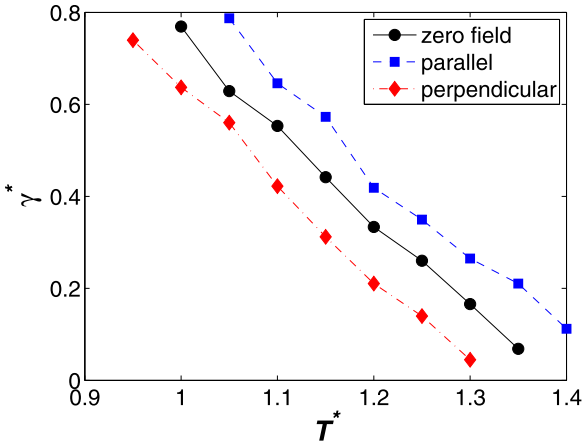

FIG. 7. (Color online) Surface tension vs temperature for $\mu^* = 1.0$ and $E^* = 0$ and 2.0. Lines are included as a guide for the eye.

B. Interfacial properties

Surface tension γ vs temperature is shown in Fig. 7. For fixed temperature, surface tension increases for parallel field, and decreases for perpendicular field. Interfacial width vs temperature is shown Fig. 8. We note that the interfacial width depends on the interfacial area due to capillary waves [36]. The interfacial width decreases for parallel field and increases for perpendicular field.

The average orientation profiles $\cos\theta(z)$ as calculated using Eqs. (10) and (11) for $\mu^* = 1.0$ are shown in Fig. 9. We remind the reader that orientation θ is calculated parallel to the field direction (not the interface), so the magnitude of orientation can be directly compared for different field directions. For a field applied parallel to the interface, the ordering in the liquid phase is greater than that in the vapor phase, while for a field applied perpendicular to the interface, the opposite is true. A similar trend was reported by Jia and Hentschke [21], albeit for constant surface potential and charge boundary conditions.

To confirm these results, bulk liquid and vapor-phase simulations using coexisting densities from the previous two-phase

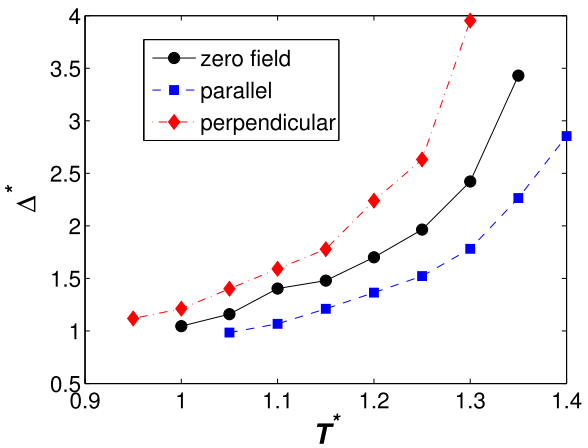

FIG. 8. (Color online) Interfacial width Δ^* for $A^* = 100$ vs reduced temperature T^* for $\mu^* = 1.0$ and $E^* = 0$ and 2.0. Lines are included as a guide for the eye.

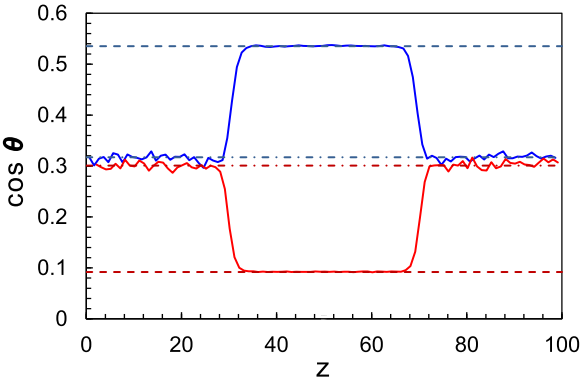

FIG. 9. (Color online) Average dipole orientation parameter $\cos\theta(z)$ vs position z at $T^* = 1.0$, for $\mu^* = 1.0$ and $E^* = 1.0$. Dashed lines are for bulk liquid system and dot-dashed lines are for bulk vapor system. The blue lines (top three lines) are for the parallel field, and the red lines (bottom three lines) are for perpendicular field. For the bulk perpendicular case, the simulation field strength is $E^* = 1.0/\epsilon$.

simulations were performed with an applied external field $E^{*\text{ext}} = 1.0$ to obtain the average liquid and vapor orientation. Simulations for bulk liquid and vapor-phase simulations with zero field were also run to obtain the dielectric constants of the liquid and vapor phases, which gave $\epsilon = 7.92$ for the liquid and $\epsilon = 1.06$ for the vapor. A third set of bulk liquid and vapor-phase simulations were then run using a reduced external field [Eq. (7)] of $E^{*\text{eff}} = 0.126$ for the liquid and $E^{*\text{eff}} = 0.941$ for the vapor to mimic polarization. As seen in Fig. 9, the orientation for the two-phase simulation with parallel field $E^*_{\parallel} = 1.0$ is in excellent agreement with the bulk simulations for $E^{*\text{ext}} = 1.0$. The orientation for the two-phase system with perpendicular field $E^*_{\perp} = 1.0$ is also in excellent agreement with the bulk systems and external field reduced by the dielectric constant $E^{*\text{eff}}$, because of the polarization that occurs when the field is perpendicular to the interface.

The connection between these two boundary conditions and the external field direction has not been made previously, but as noted above (cf. Fig. 5) the ΔT^*_c data implies that the constant surface potential boundary condition is equivalent to a parallel field and the constant surface charge boundary condition is equivalent to a perpendicular field. Further confirmation of these equivalences is given by orientation data for different fields shown in Fig. 9. These results are consistent with the parallel field direction resulting in no polarization which is equivalent to the constant surface potential. Hence simply applying an external field in a GEMC simulation corresponds to a field applied parallel to the interface and to a constant surface potential boundary condition. The connection between the boundary condition and the direction of the applied field is the nature of the polarization as discussed in the text concerning Eq. (7). When the field is applied perpendicular to the interface, the density in the direction of the field changes at the interface, and the polarization occurs at the interface. This polarization reduces the external field of the fluid by a factor equal to the static dielectric constant (for the conditions shown in Fig. 9) and corresponds to a constant surface charge boundary condition. For this reason, bulk simulations of the dipolar liquid must use the reduced field to be equivalent to

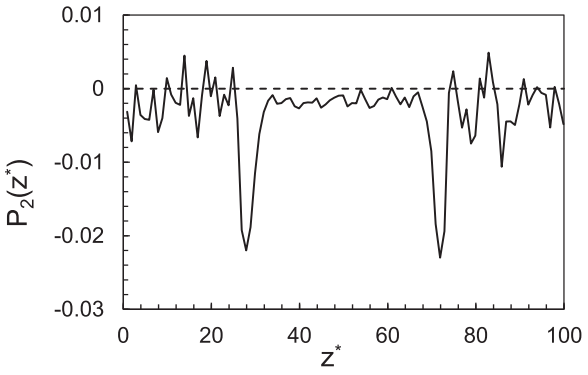

FIG. 10. Orientation profile $P_2(z^*)$ vs position z^* for $E^* = 0$, $\mu^* = 2.5$, and $T^* = 2.2$. The dashed line at $P_2(z^*) = 0$ is included as a guide for the eye.

the perpendicular field case with an interface as shown in Fig. 9. For the parallel field case, the density does not change in the direction of the field and the field is not altered by polarization. Thus this corresponds to the constant potential boundary condition.

Even for zero external field, some ordering still occurs near the interface as shown in Fig. 10. This effect was also observed in simulations of Stockmayer fluids by Mecke *et al.* [40]. The effect is small in magnitude, but the difference between the interface and bulk regions is clearly distinguishable in our simulations too.

Average orientation $\cos\theta$ vs external field strength for $\mu^* = 1.0$, and $T^* = 1.2$ for both liquid phase and vapor phases is shown in Fig. 11. The difference in orientation for parallel vs perpendicular fields for a given field strength is

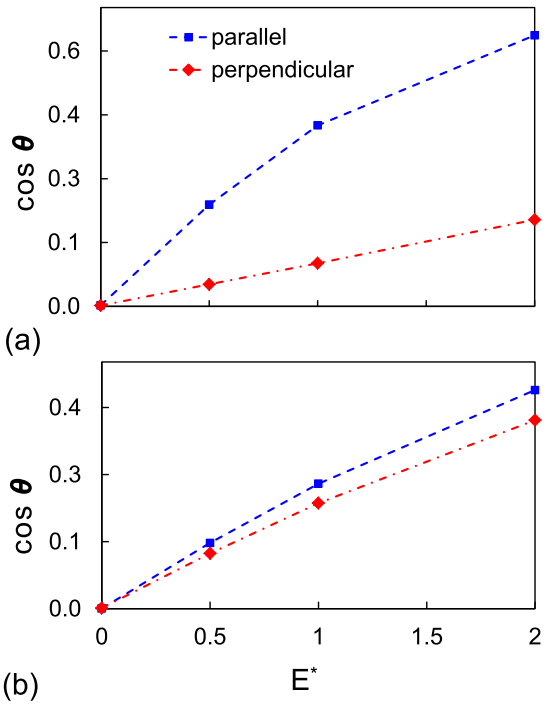

FIG. 11. (Color online) Average orientation $\cos\theta$ vs external field strength for $\mu^* = 1.0$ and $T^* = 1.2$ for (a) liquid and (b) vapor phase. The lines are included as a guide for the eye.

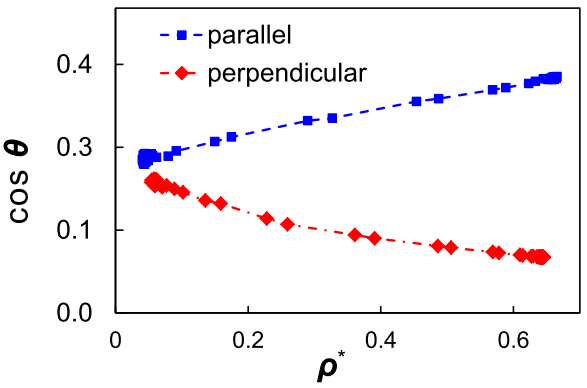

FIG. 12. (Color online) Orientation profile of average $\cos\theta(\rho^*)$ vs ρ^* for $E^* = 1.0$, $\mu^* = 1.0$, and $T^* = 1.2$. The lines are included as a guide for the eye.

greater for the liquid than for the vapor. The variation of the orientation $\cos\theta(z)$ within the interfacial region vs density for $\mu^* = 1.0$ and $T^* = 1.2$ is shown in Fig. 12. For parallel field, the orientation increases with density, while it decreases for perpendicular field due to the density dependence of the dielectric constant. A similar dependence of the orientation on the density was reported previously for the corresponding boundary conditions (see Fig. 9 of Ref. [21]).

IV. CONCLUSION

By performing molecular-dynamics simulations explicitly treating the liquid-vapor interface for a Stockmayer fluid, we determined the effect of an external field magnitude and direction on the properties of the coexisting phases. In a field perpendicular to the interface, we find that the critical temperature decreases, the surface tension decreases, and the interfacial width increases. For the field parallel to the interface, the change is opposite to the perpendicular case. The orientational order in the liquid and vapor phases depends on the field direction and exhibits a polarization effect for perpendicular fields. The alignment of the dipoles in the liquid is *less* than in the vapor phase for perpendicular fields, because of the polarization which produces an alignment in the liquid phase equal to the alignment in a bulk liquid with field E/ϵ (at least for the conditions shown in Fig. 9). In the parallel case, there is no polarization effect and the order in the liquid phase is larger than in the vapor phase.

These results help explain many of the differences found in previous theoretical works. Our results show that applying an external field to a GEMC simulation corresponds to a field parallel to the interface resulting in an increase in T_c with field. Comparison with simulations of Jia and Hentschke [21] show that their boundary conditions of fixed potential and charge density correspond to parallel and perpendicular field directions, respectively. The results also lay a foundation for understanding experimental data by treating a well-defined dipolar system. Insofar as the experimental system is well modeled by the Stockmayer fluid, our results should agree with experimental data (e.g., the sign of the change in T_c), such as for pure SF_6 [6]. However, most experiments on polar liquids have been for liquid mixtures [2–4,8], and additional factor(s) can alter the sign of the change in T_c [53]. For

more complicated experimental systems, our results provide a base for understanding the effect of additional characteristics beyond the simple dipolar model.

ACKNOWLEDGMENTS

This work was performed at the Center for Integrated Nanotechnologies, a U.S. Department of Energy, Office of Basic Energy Sciences user facility. Sandia National Laboratories is a multiprogram laboratory managed and operated by Sandia Corporation, a wholly owned subsidiary of Lockheed Martin Corporation, for the U.S. Department of Energy's National Nuclear Security Administration under Contract No. DE-AC04-94AL85000.

APPENDIX: EWALD SLAB CORRECTION

To simulate a planar interface of the Stockmayer fluid, one could use a 2D Ewald sum along with nonperiodic boundary conditions (for example, specular reflecting walls) in the direction normal to the interface. However, the 2D Ewald sum is much more expensive than the 3D Ewald sum [27], and using nonperiodic boundary conditions can lead to artifacts. Mecke *et al.* studied the Stockmayer fluid in zero field and found that the 3D Ewald sum is equivalent to the 2D Ewald sum if the spacing between slabs is sufficiently large [40]. However, for systems with a net dipole in the direction normal to the interface (i.e., when an external field is applied perpendicular to the interface) periodically repeated slabs produce spurious electric fields, much like a stack of parallel plate capacitors [27], which can erroneously influence the orientation of the point dipoles. A slab correction [28,29] can be included to reduce this undesirable effect.

The correction term for an infinitely thin slab is [28,29]

$$U^{\mathrm{c}} = -\frac{2\pi}{V} M_z^2, \tag{A1}$$

where M_z is the total dipole moment in the z direction:

$$M_z = \sum_{i=1}^{N} \mu_i. \tag{A2}$$

The spurious field due to periodically repeated slabs is approximated by

$$E_z^{\mathrm{c}} = -\frac{\partial U^{\mathrm{c}}}{\partial \mu_{z,i}} = \frac{4\pi}{V} M_z. \tag{A3}$$

Because this field is uniform (nonspatially varying), there is no net force on the dipole, but there is a torque:

$$\mathbf{T}_i^{\mathrm{c}} = \boldsymbol{\mu}_i \times \mathbf{E}^{\mathrm{c}}, \tag{A4}$$

and therefore $T_{z,i}^{\mathrm{c}} = 0$,

$$T_{x,i}^{\mathrm{c}} = \frac{4\pi}{V} M_z \mu_{y,i} \tag{A5}$$

and

$$T_{y,i}^{\mathrm{c}} = -\frac{4\pi}{V} M_z \mu_{x,i}. \tag{A6}$$

Subtracting the above corrections for energy and torque from the respective system energy and torque is termed the Ewald *slab correction* in this work.

TABLE II. Approximate size of vapor and liquid regions for the simulations.

Simulation	Vapor size	Liquid size
1	50	25
2	100	50
3	50	50
4	100	25
5	200	25

The slab correction term is a first-order correction that gives the correct limiting behavior for an infinitely thin slab. However, it has been shown that including this lowest-order term and inserting a layer of empty volume that makes the interslab spacing three to five times larger than the thickness of the slab is sufficient [27]. In order to reduce artifacts from using a reflecting wall, the thickness of the vapor region (which has a low density and acts similar to a region of vacuum) was increased relative to that of the liquid, and periodic boundary conditions were used instead. Simulations (see below) show this to be reasonable.

A series of simulations were run in which the thickness of the vapor and liquid phases was varied as shown in Table II, with $\mu^* = 1.0$, $T^* = 1.0$, and $E_\perp^* = 1.0$. The simulation cell size was $L_x^* = L_y^* = 9$ with L_z^* given by summing the approximate liquid and vapor sizes in Table II. The real-space cutoff for the Ewald sum was $r_{\mathrm{cut}} = 6.0\sigma$, and Ewald parameters were adjusted to give a relative rms force error of approximately 10^{-5} as predicted by formulas given in Ref. [23] relative to a force of 1.0 LJ units. Neglecting the slab correction when there is a net dipole moment in the z direction (i.e., for perpendicular field) causes the liquid phase orientation to be highly dependent on the system size, but including the slab correction greatly reduces this dependence as shown in Fig. 13 and also gives excellent agreement with a bulk simulation at liquid density with $E^* = 1.0/\epsilon$ (cf. Fig. 9). The Ewald slab correction was therefore used for all other two-phase simulations shown in this work.

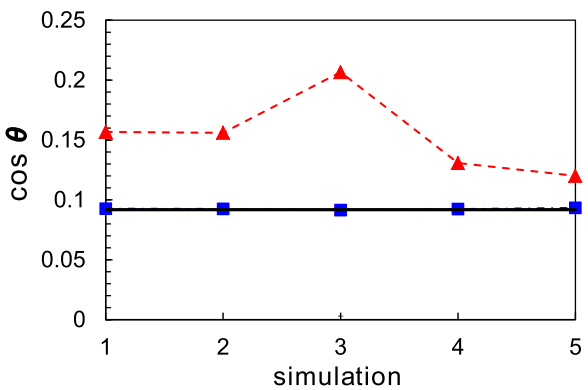

FIG. 13. (Color online) Liquid orientation for varying size of liquid and vapor regions, with $\mu^* = 1.0$, $T^* = 1.0$, and $E_\perp^* = 1.0$ with (blue squares) and without (red triangles) the Ewald slab correction. Orientation for a bulk simulation at liquid density with $E^* = 1.0/\epsilon$ (cf. Fig. 9) is also shown (solid black line).

[1] D. Wei and G. N. Patey, Phys. Rev. Lett. **68**, 2043 (1992).
[2] P. Debye and K. Kleboth, J. Chem. Phys. **42**, 3155 (1965).
[3] K. Orzechowski, Chem. Phys. **240**, 275 (1999).
[4] D. Beaglehole, J. Chem. Phys. **74**, 5251 (1981).
[5] K. Orzechowski, M. Adamczyk, A. Wolny, and Y. Tsori, J. Phys. Chem. B **118**, 7187 (2014).
[6] J. Hegseth and K. Amara, Phys. Rev. Lett. **93**, 057402 (2004).
[7] L. Landau and E. Lifshitz, *Electrodynamics of Continuous Media* (Pergamon Press, New York, 1960).
[8] K. Orzechowski, M. Kosmowska, and M. Adamczyk, J. Phys. Chem. B **116**, 2492 (2012).
[9] S. Samin and Y. Tsori, J. Phys. Chem. B **115**, 75 (2011).
[10] S. Stepanow and T. Thurn-Albrecht, Phys. Rev. E **79**, 041104 (2009).
[11] R. Srivastava, J. K. Singh, and P. T. Cummings, J. Phys. Chem. C **116**, 17594 (2012).
[12] K. A. Maerzke and J. I. Siepmann, J. Phys. Chem. B **114**, 4261 (2010).
[13] D. Boda, I. Szalai, and J. Liszi, J. Chem. Soc., Faraday Trans. **91**, 889 (1995).
[14] D. Boda, J. Winkelmann, J. Liszi, and I. Szalai, Mol. Phys. **87**, 601 (1996).
[15] M. E. Van Leeuwen, B. Smit, and E. M. Hendriks, Mol. Phys. **78**, 271 (1993).
[16] M. J. Stevens and G. S. Grest, Phys. Rev. E **51**, 5976 (1995).
[17] K. Kiyohara, K. E. Gubbins, and A. Z. Panagiotopoulos, J. Chem. Phys. **106**, 3338 (1997).
[18] K. Kiyohara, K. J. Oh, X. C. Zeng, and K. Ohta, Mol. Simul. **23**, 95 (1999).
[19] V. B. Warshavsky and X. C. Zeng, Phys. Rev. E **68**, 051203 (2003).
[20] I. Szalai and S. Dietrich, J. Phys.: Condens. Matter **20**, 204122 (2008).
[21] R. Jia and R. Hentschke, Phys. Rev. E **80**, 051502 (2009).
[22] W. H. Stockmayer, J. Chem. Phys. **9**, 398 (1941).
[23] Z. Wang and C. Holm, J. Chem. Phys. **115**, 6351 (2001).
[24] M. P. Allen and D. J. Tildesley, *Computer Simulation of Liquids* (Oxford University Press, New York, 1989).
[25] A. Toukmaji, C. Sagui, J. Board, and T. Darden, J. Chem. Phys. **113**, 10913 (2000).
[26] R. Pollock and B. Alder, Physica A **102**, 1 (1980).
[27] D. Frenkel and B. Smit, *Understanding Molecular Simulation: From Algorithms to Applications*, 2nd ed. (Academic Press, New York, 2002).
[28] I.-C. Yeh and M. L. Berkowitz, J. Chem. Phys. **111**, 3155 (1999).
[29] S. H. L. Klapp and M. Schoen, J. Chem. Phys. **117**, 8050 (2002).
[30] L. Onsager, J. Am. Chem. Soc. **58**, 1486 (1936).
[31] J. Barker and R. Watts, Mol. Phys. **26**, 789 (1973).
[32] N. Karasawa and W. A. Goddard, J. Phys. Chem. **93**, 7320 (1989).
[33] J. López-Lemus and J. Alejandre, Mol. Phys. **100**, 2983 (2002).
[34] P. J. in 't Veld, A. E. Ismail, and G. S. Grest, J. Chem. Phys. **127**, 144711 (2007).
[35] B. Smit, J. Chem. Phys. **96**, 8639 (1992).
[36] A. E. Ismail, G. S. Grest, and M. J. Stevens, J. Chem. Phys. **125**, 014702 (2006).
[37] M. Mecke, J. Winkelmann, and J. Fischer, J. Chem. Phys. **107**, 9264 (1997).
[38] J. G. Kirkwood and F. P. Buff, J. Chem. Phys. **17**, 338 (1949).
[39] J. G. Harris, J. Phys. Chem. **96**, 5077 (1992).
[40] M. Mecke, J. Fischer, and J. Winkelmann, J. Chem. Phys. **114**, 5842 (2001).
[41] P. I. C. Teixeira and M. M. T. da Gama, J. Phys.: Condens. Matter **14**, 12159 (2002).
[42] S. Plimpton, J. Comput. Phys. **117**, 1 (1995).
[43] T. Schneider and E. Stoll, Phys. Rev. B **17**, 1302 (1978).
[44] B. Dünweg and W. Paul, Int. J. Mod. Phys. C **02**, 817 (1991).
[45] J. Rowlinson and F. Swinton, *Liquids and Liquid Mixtures* Butterworth's Monographs in Chemistry (Butterworth Scientific, London, 1982).
[46] A. Pelissetto and E. Vicari, Phys. Rep. **368**, 549 (2002).
[47] B. Smit, C. Williams, E. Hendriks, and S. D. Leeuw, Mol. Phys. **68**, 765 (1989).
[48] N. B. Wilding, Phys. Rev. E **52**, 602 (1995).
[49] N. B. Wilding, J. Phys.: Condens. Matter **9**, 585 (1997).
[50] K. Binder, Mol. Phys. **108**, 1797 (2010).
[51] J. J. Potoff and A. Z. Panagiotopoulos, J. Chem. Phys. **109**, 10914 (1998).
[52] J. Bartke, Ph.D. thesis, University of Wuppertal, 2008.
[53] Y. Tsori, Rev. Mod. Phys. **81**, 1471 (2009).